Preparation and Characterization of Mesoporous Activated Carbon-Supported Tin Oxide Nanocomposites from Agro-Waste (*Cyperus Corymbosus Grass Stem*) and its Use as a Highly Efficient Catalyst in a Three-component Reaction

Stanelybritto MARIA ARUL FRANCIS [1], Sharmil Suganya RAJAN BABU [2], Venugopal THIRUVENGADAM [*]

[1] *Department of Chemistry, Government College of Engineering, Salem -636011, Tamil Nadu, India*
[2] *Department of Electrical and Electronics Engineering, Government College of Engineering, Salem -636011, Tamil Nadu, India*

http://doi.org/10.5755/j02.ms.37968

Received 9 July 2024; accepted 14 October 2024

The present study reports an eco-friendly preparation of mesoporous carbon-supported tin oxide nanocomposite from agro-waste (*Cyperus corymbosus* grass stem). The CCSAC - SnO_2 prepared by greener method successfully utilizing *Cyperus corymbosus* waste. The prepared CCSAC-SnO_2 nanocomposite was characterized using advanced analytical techniques such as Fourier Transform Infrared spectroscopy (FTIR), X-ray diffraction analysis (XRD), Field Emission Scanning Electron Microscopy (FE-SEM), Raman spectroscopy, Brunauer-Emmett-Teller (BET) analysis, X-ray photoelectron spectroscopy (XPS) analysis, and Thermogravimetry Differential Thermal Analysis (TG-DTA). The amorphous and crystalline nature of *Cyperus corymbosus* stem-activated carbon (CCSAC) and *Cyperus corymbosus* activated carbon supported tin oxide nanocomposites (CCSAC-SnO_2 nanocomposite) was confirmed using powder XRD analysis. FT-IR analysis was used to identify the surface functional groups attached to the CCSAC and CCASC-SnO_2 nanocomposite. The element composition of CCSAC and CCSAC-SnO_2 nanocomposite was confirmed by EDX analysis. BET analysis confirmed the CCSAC-SnO_2 nanocomposite mesoporous nature. XPS and TG-DTA analysis confirmed the elemental composition and thermal stability of the CCSAC-SnO_2 nanocomposite. The CCSAC-SnO_2 nanocomposite was used as a nanocatalyst in a three-component reaction. This study highlights the potential of utilizing plant waste to prepare valuable mesoporous CCSAC-SnO_2 nanocomposite, highlighting both environmental sustainability and catalytic efficiency.
Keywords: mesoporous activated carbon, cyperus corymbosus, three-component reaction, nano-catalyst, SnO_2

1. INTRODUCTION

In recent years, biomass from waste products, agricultural residue, and agro-based industries worldwide has been claimed to be included in the eco-friendly source of carbon precursors. [1] The transformation of agro-waste into carbon-based products is both environmentally friendly and promising. Carbon material derived from biomass can be used in various applications, including water treatment, catalyst, catalyst support, hydrogen storage, and CO_2 capture. With its large surface area, activated carbon (AC) is utilized to support catalysts in heterogeneous catalysis. Specifically, porous AC is the most commonly employed material since it easily archives very high catalyst dispersions and strong catalytic activity [2]. Conventional heterogeneous catalysts often exhibit poor catalytic activity due to the limited accessibility of reactants to active sites. [3]. However, this limitation can be overcome by utilizing carbon, which disperses the catalyst [4, 5, 6]. Recently, carbon-based materials have been used as catalysts as they offer several advantages such as good stability in acidic and basic mediums, good thermal stability, ease of availability compared to conventional catalysts, and easy recoverability from reaction mixtures [7, 8], due to their higher surface area and porosity compared to traditional catalyst supports such as alumina and silica [9, 10, 11].

A heterogeneous acid catalyst is better than a homogeneous acid catalyst because of its reusability, ease of separable from the reaction mixture, selectivity, environmental friendliness, and cost-effectiveness [12]. Acid catalysts are among the most important types used in chemical industry reactions. Reactions such as Friedel crafts acylation and alkylation, aromatic nitration, isomerization, and halogenation are typically catalyzed by H_2SO_4, or Lewis's acids like BF_3 and $AlCl_3$ [13]. These reagents are toxic and difficult to separate producing toxic and corrosive waste [14]. The development of eco-friendly sustainable heterogeneous acid catalysts aims to overcome these problems [15]. Organic transformation using nanocatalysts has been a rapidly emerging trend for decades and is crucial in the area of sustainable chemistry [16]. Among nanoparticles, SnO_2 is notable due to its unique properties. SnO_2 is highly stable, optical transparency, and thermal stable [17, 18, 19]. Due to its excellent acidic properties, it acts as an effective heterogeneous catalyst in organic reactions [20].

Cyperus corymbosus grass stems produced in the local mat-making industry, Tiruchirappalli were used as biomass for the preparation of activated carbon through

[*] Corresponding author. Tel.: +91-93-81325813.
E-mail: *venugopalt@gcesalem.edu.in* (V. Thiruvengadam)

carbonization under an inert atmosphere [21]. *Cyperus corymbosus* grass is cultivated extensively in Tiruchirappalli district, Tamil Nadu for mat production. A survey reported that approximately 14 tons per hectare of korai waste produced in this area per harvest is typically burnt [22]. Burning of such large quantities of biomass from the two annual harvests would lead to environmental problems [23].

In general, SnO_2 nanoparticles have been produced using various chemical, physical and green methods including hydrothermal [24], sol-gel [25], precipitation [26], thermal decomposition [27], mechanochemical [28], micro-microemulsion methods [29]. The methods for the preparation of nano tin oxide involve the use of various chemical solvents, reagents, and surfactants, in chemical methods, which creates a serious environmental impact and health hazards [30]. In contrast, the physical methods are challenging due to the requirement for high temperature and pressure, complex equipment, and skilled manpower [31]. Therefore, it is highly important to develop methods that are eco-friendly, efficient, cost-effective, and greener. Many researchers have to focus on developing green methods for preparing tin oxide nanoparticles as a solution. In green chemistry strategies, plants and micro-organisms, can be used as alternatives to conventional physical and chemical methods [32]. The plant-mediated preparation of nanoparticles is preferable to conventional methods because it is free from toxic chemicals and acts as a natural capping agent as well reducing agent. Additionally, plant-mediated preparation of nanoparticles is eco-friendly and straightforward, requiring no high temperature and pressure or costly equipment, and results in stable nanoparticles with varying sizes and shapes [33, 34].

Multicomponent reactions (MCRs) are efficient and high bond-forming methods in organic synthesis [35] to produce heterocyclic compounds with cost benefits such as minimal purification process, reduced operational steps, and single reaction conditions. [36] Tetrahydrobenzo[b]pyrans units, found in many natural products, synthetic origin [37] has considerable biological and pharmacological properties such as diuretic, spasmolytic [38], anti-HIV [39], apoptosis inducer [40], antitubercular [41], antifungal [42], antibacterial, anticancer [43], anti-inflammatory properties [44]. Tetrahydrobenzo[b]pyrans are synthesized through a three-component reaction involving cyclic 1,3-diketones, aldehydes, and malononitrile in the presence of various homogeneous and heterogeneous acid/base catalysts such as KF/Alumina [45] silica gel-supported polyphosphoric acid [46] hexadecyl trimethyl ammonium bromide (HTMAB) [47], guanidine supported on magnetic nanoparticles Fe_3O_4 [48], Silica-bonded S-sulfonic acid (SBSSA) [49], magnesium oxide (MgO) [50], triethanolamine [51], 4-dimethylaminopyridine (DMAP) under microwave conditions [52] and L-proline [53]. However, these methods have drawbacks such as tedious catalyst preparation, toxic and expensive reagents, odorous catalysts, non-recyclable catalysts, long reaction times, and extensive manpower requirements for work-up procedures [54]. Therefore, the development of a greener and more efficient catalyst in the synthesis of Tetrahydrobenzo[b]pyrans could overcome these drawbacks.

To address drawbacks, this work is to develop an effective, eco-friendly, and cost-effective heterogeneous catalyst for various organic transformations and MCRs. Specifically, the preparation of CCSAC-SnO_2 nanocomposite from agricultural waste used as a catalyst in synthesizing Tetrahydrobenzo[b]pyrans is reported.

2. MATERIALS AND METHODS

2.1. Chemicals and materials

Tin chloride pentahydrate was purchased from Loba Chemie Pvt. Ltd, India. *Cyperus corymbosus* (korai grass) was collected from local mat manufacturers in Tiruchirappalli, Tamil Nadu, India. The tubers of *Ruellia tuberosa* were collected from farmland in Salem, Tamil Nadu, India. 4-nitro benzaldehyde, malononitrile, and dimedone were purchased from Sigma-Aldrich Chemicals Private Limited. TLC plates, Silica gel 60 F_{254} was purchased from Sigma-Aldrich Chemicals Private Limited.

2.2. Preparation of CCSAC-SnO_2 nanocomposite. Preparation of activated carbon from *Cyperus corymbosus* stem (CCSAC)

Activated carbon was prepared from the waste of *Cyperus corymbosus* (korai grass) stems by using a method Ting Zhang *et al*., with a slight modification [55]. Firstly, the dried *Cyperus corymbosus stem* (CCS) was chopped into small pieces, washed with distilled water (DW), and dried at 80 °C for 10 hours. The fully dried CCS pieces were soaked in 1 M KOH for 24 hours, then filtered, and dried at 80 °C for 10 hours. The fully dried CCS pieces were carbonized in a muffle furnace for about 3 hours at 700 °C an inert atmosphere. After washing the carbonized CCS with 1 M HCl, it was then dried at 80 °C for 5 hours. Finally, KOH was successfully removed to obtain CCSAC.

2.3. Preparation of CCSAC-SnO_2 nanocomposite. Preparation of *Ruellia tuberosa* fresh root extract

About 50 grams of fresh *Ruellia tuberose* root were chopped into small pieces, transferred to a 500 ml beaker containing DW, and boiled for 2 hours. After boiling, the extracts were filtered using filter paper, and stored in a refrigerator for further use.

2.4. In situ preparation of CCSAC-SnO_2 nanocomposite catalyst

0.1 M of stannous chloride (500 ml) was stirred with a magnetic stirrer at room temperature. After one hour, 100 ml of *Ruellia tuberose* root extracts were added drop by drop to the solution, and then the temperature was increased to 60 °C [56]. A white precipitate was formed, and 0.2 grams of CCSAC was added to the solution. The entire mixture was stirred for about 4 hours, during which water evaporated, and the remaining residue calcinated in the furnace at about 700 °C for three hours.

2.5. Catalytic activity. General procedure of the three-component reaction

A mixture of 4-nitro benzaldehyde (1) (1 mmol), malononitrile (2) (1.06 mmol), and dimedone (3) (1 mmol), ethanol 2 mL were refluxed and stirred. Thereafter,

CCSAC-SnO_2 nanocomposite (0.3 mg) was added as a nanocatalyst. The progress of the reaction was monitored by Thin Layer Chromatography (TLC) using ethyl acetate and hexane (3:4) as eluent. Upon completion of the reaction, the obtained solid was recrystallized in ethanol.

3. CHARACTERIZATION

The surface was analyzed by using FT-IR spectroscopy (IR Affinity-1, Shimadzu, Japan, IIT Jammu) employing the KBr pellet method. XRD was tested using a Rigaku Dmax-rc X-ray diffractometer with Ni-filtered Cu Kα (λ = 1.54059 ˚A) radiation at IIT- Jammu. Morphology was examined using a Field Emission Scanning Electron Microscope (FESEM) (FESEM, JSM 7900F, JEOL) at the Central Instrumentation Facility (SAPTARSHI), IIT Jammu. Energy dispersive X-ray analysis was carried out by SEM-EDS (TESCAN BRNO, 62300) to analyze the elemental composition. Raman spectra were analyzed using a Raman spectrometer (RENISHAW, UKRENISHAW BASIS SERIES WITH 514 LASERS, at the Sophisticated Analytical Instrumentation Centre (SAIC), Tezpur University). Porous size and surface area were analyzed using a Brunauer-Emmett-Teller method (BET), (Quantachrome Corporation) at the Material Analysis, and Research Centre, Bengaluru. X-ray Photo-electron Spectroscopy was obtained using a Thermos Scientific, NEXA Surface analyzer, CIF, IIT, Jammu. Thermo gravimetric/differential thermal analysis was conducted at SAIF, Roorkee (EXSTAR, SII 6300 EXSTAR). Proton nuclear magnetic resonance (^{1}H NMR) spectra were recorded using a Bruker Avance III 400 MHz spectrometer at the Vellore Institute of Technology, India.

4. RESULTS AND DISCUSSION

4.1. IR analysis of CCSAC and CCSAC-SnO_2 nanocomposite

The FT-IR spectrum of CCSAC is presented in Fig. 1 The absorption band at approximately ~ 3451 cm^{-1} is attributed to O-H stretching vibrations of hemicellulose, absorbed water molecules, pectin, lignin, and cellulose. Absorption bands at ~ 2920 cm^{-1} and ~ 2854 cm^{-1} are observed due to C-H stretching vibrations in the lignin polysaccharides, such as hemicellulose and cellulose [57]. The peak at ~ 1384 cm^{-1} is assigned to the bending vibrations of $–CH_3$ and the C=O stretch is due to the carbonyl group.

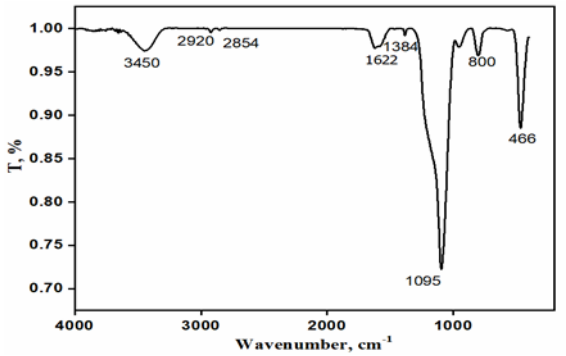

Fig. 1. FT-IR spectrum of CCSAC

The vibration peak appearing near ~ 800 – 600 cm^{-1} belongs to the peak of bending out of the plane C–H [58].

Fig. 2 shows the FT-IR spectrum of CCSAC-SnO_2 nanocomposite with some characteristic major vibrational frequencies at ~ 3411 cm^{-1} related to free OH peaks. The peaks around ~ 850 cm^{-1} and ~ 541 cm^{-1} are assigned to Sn-O-Sn stretching mode due to surface bridging oxide formed by the condensation of adjacent surface hydroxyl groups. The presence of these characteristic bands confirms the formation of SnO_2 nanocomposite [59].

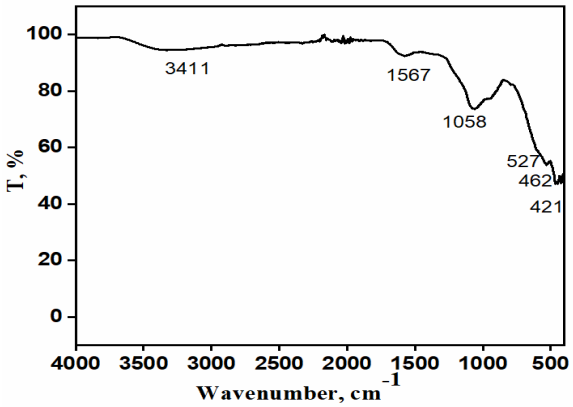

Fig. 2. IR spectrum of CCSAC-SnO_2 nanocomposite

4.2. XRD analysis of CCSAC and CCSAC-SnO_2NPs

The chemical composition of CCSAC was analyzed using XRD analysis. Fig. 3 displays the XRD patterns of CCSAC, which show two peaks at ~ 24.2 and ~ 43.2. These peaks are assigned to the (002) and (100) planes of crystalline carbon in the samples (JCPDS 00-041-1487), indicating the predominance of carbon in the hexagonal phase. Additionally, a broad amorphous region is observed in the range of 2θ = 20° [60, 61]. The average grain size of the carbon was calculated by the Scherrer equation, $D = K\lambda/(\beta\cos\theta)$ where K = 0.89 is the shape factor, k is the X-ray wavelength of CuKa radiation (0.15406 nm), h is the Bragg angle, and b is the experimental full width at half maximum (FWHM) of the respective diffraction peak (in units of radians). Using the Scherrer formula, the average grain size CCSAC is approximately 7 nm.

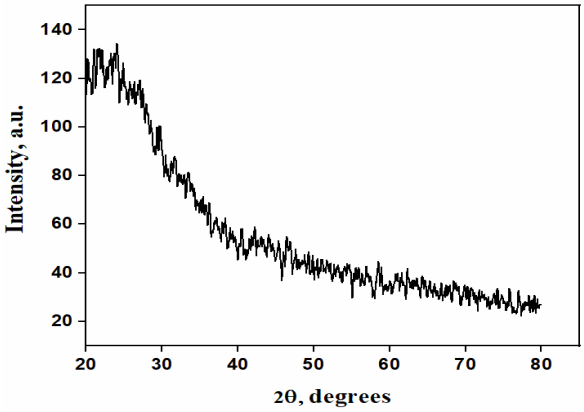

Fig. 3. XRD pattern of CCSAC

The XRD of the CSAC-SnO_2 nanocomposite, as shown in Fig. 4, exhibits four well-distinguished peaks located at

2θ = 26.7°, 33.9°, 38.1°, and 51.8°. These peaks correspond to the (110), (101), (200), and (211) reflection planes of a tetragonal SnO_2, respectively, as indicated by the standard data file (JCPDS No. 41-1445). All the indexed peaks corresponded to pure tetragonal SnO_2 and are in good agreement with the standard card. Notably, the characteristic peak of carbon at 24.2° not be observed in the CCSAC-SnO_2 nanocomposite, as it overlaps with the peak corresponding (110) plane of SnO_2 nanoparticle in the composite. [62] The very small size of the tin oxide nanoparticle is indicated by the broadening and low intensity of the peaks. The average crystalline size of the CCSAC-SnO_2 nanocomposite is approximately 2 nm. Nanocomposites with small grain size (2 nm) have a very high surface area to volume ratio. The high surface area provides a more active site for the catalytic reaction, which can significantly enhance catalytic activity.

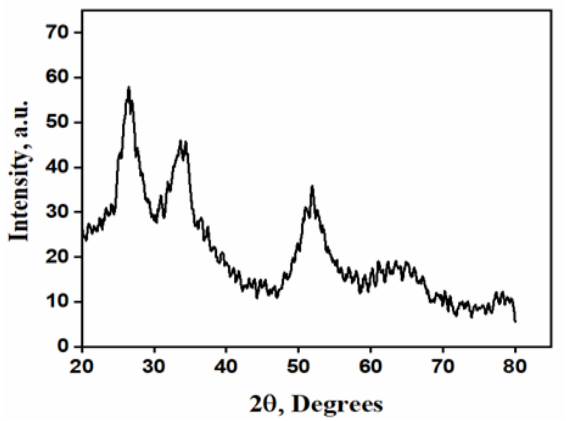

Fig. 4. XRD pattern of CCSAC-SnO_2 nanocomposite

4.3. FE-SEM images of CCSAC-SnO_2 nanocomposite

The morphologies of the CCSAC-SnO_2 nanocomposite were observed by FE-SEM, as shown in Fig. 5.

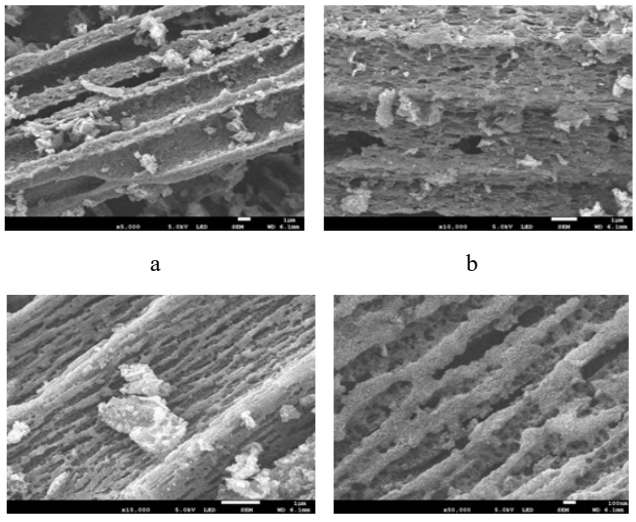

Fig. 5. FE-SEM images of CCSAC: a – 5,000; b – 10,000; c – 15,000; d – 50,000

The images reveal a non-homogeneous distribution of particles with a minimum particle size of 100 nm, indicating significant agglomeration. The prepared CCSAC exhibits a particle size within the nanometre range and resembles straw with a porous. The FESEM images of CCSAC at different kV and magnification Fig. 5 a at 5,000, b at 10,000, c at 15,000, and d at 50,000 respectively. The morphologies of the CCSAC-SnO_2 nanocomposite were observed using FE-SEM, as illustrated in Fig. 6.

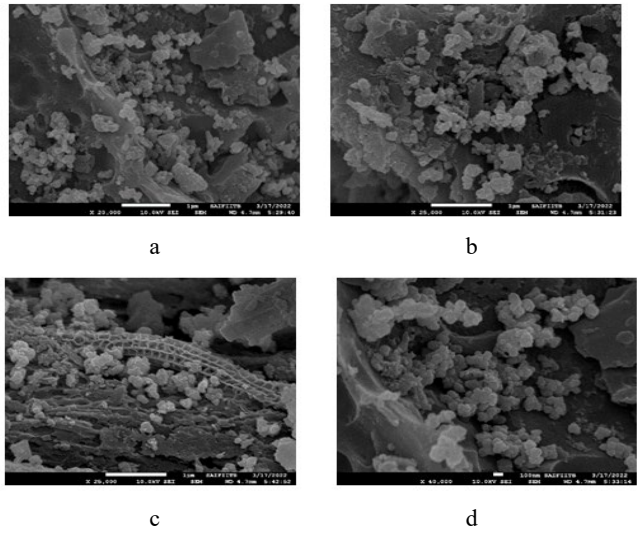

Fig. 6. FE-SEM images of CCSAC-SnO_2 composite: a – 20,000; b – 25,000; c – 25,000; d – 40,000

The FESEM images of the CCSAC-SnO_2 nanocomposite were captured at different kV and magnifications Fig. 5 a at 20,000, b at 25,000, c at 25,000, and d at 40,000 respectively. The images indicate a non-homogeneous distribution of particles, within a minimum particle size of approximately 100 nm in Fig. 5 d where most particles appear agglomerated. The size of the prepared CCSAC-SnO_2 nanocomposite suggests that the particle is within a nanometer range and exhibits a porous structure resembling straw. Because the preparation of CCSAC-SnO_2 did not alter the CCSAC morphology, it indicated the stability of carbon. It also makes this nanocomposite well-stable during the catalytic process.

4.4. EDX analysis of CCSAC and CCSAC-SnO_2 nanocomposite

The elemental composition of CCSAC and CCSAC-SnO_2 nanocomposite was analyzed using the energy-dispersive X-ray analysis as shown in Fig. 7. The EDX spectrum of CCSAC displayed sharp peaks corresponding to oxygen (O) and carbon (C) along with some trace amounts of silica. The presence of silica indicates that *Cyperus corymbosus* plant is one of the silica accumulators [63]. In the case of the CCSAC-SnO_2 nanocomposite, the intensity of the oxygen peak is notably higher than that in CCSAC, which can be attributed to the presence of SnO_2. This indicates an increased oxygen content in nanocomposite due to the incorporation of tin oxide nanoparticles.

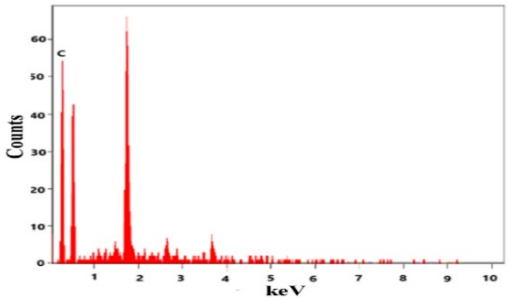

a

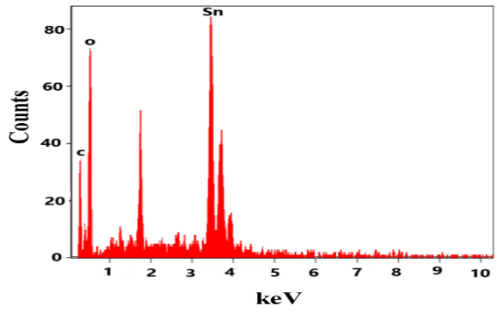

b

Fig. 7. a – EDX spectrum of CCSAC; b – EDX spectrum of CCSAC-SnO_2 nanocomposite

4.5. Raman spectra of CCSAC and CCSAC-SnO_2 nanocomposite

Fig. 8 shows the Raman spectra of CCSAC. The G band was observed at 1590 cm^{-1}, D band appeared at a Raman shift of 1359 cm^{-1}. The G band corresponds to the in-plane stretching of the sp^2 carbon-carbon bond in the CCSAC. D band indicates the amorphous regions within the activated carbon. The G and D bands suggest the CCSAC contains both amorphous and ordered graphite regions in carbon structures. The intensity of the G band is notably higher than that of the D band, indicating a more ordered structure.

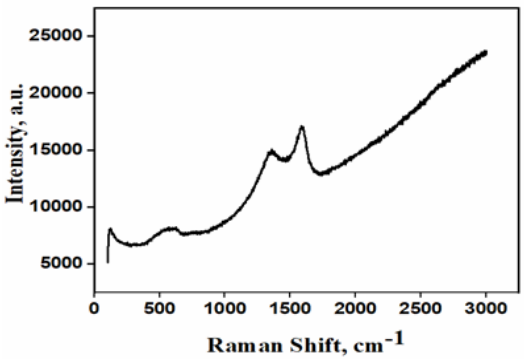

Fig. 8. Raman spectrum of CCSAC

Raman spectra of the CCSAC-SnO_2 nanocomposite are shown in Fig. 9. In general, the distorted (D), and graphite (G) bands are the two characteristics of carbon. The D band commonly appears in the range of 1300 – 1400 cm^{-1} and is associated with distorted or amorphous carbon while the G band is strong, and usually appears in the range 1565 – 1595 cm^{-1}. The G band arises from the plane tangential stretching of C-C bonds in carbon. The characteristic four major Raman modes originated from SnO_2 nanoparticles which are designated as A_{1g}, B_{1g}, B_{2g}, and E_g [64]. The peak at 476.5 cm^{-1} assigned to E_g mode is related to the vibration of oxygen in the plane. The Raman peaks at 631 and 768 cm^{-1} can be attributed to the A_{1g} and $B_{2\,g}$ symmetry vibration modes of Sn-O bonds [65].

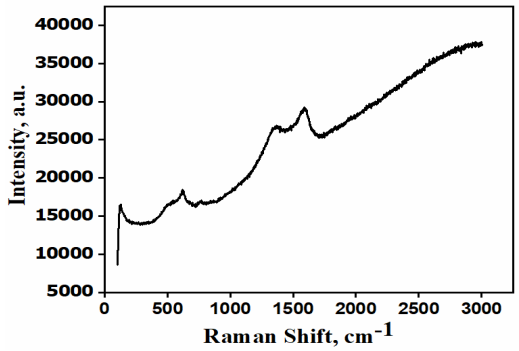

Fig. 9. Raman spectrum of CCSAC-SnO_2 nanocomposite

4.6. BET analysis of CCSAC-SnO_2 nanocomposite

In Fig. 10, the Brunauer-Emmett-Teller (BET) method is utilized to determine the specific surface area, pore volume, and pore diameter of the CCSAC-SnO_2 nanocomposite. According to the N_2 adsorption-desorption isotherms, CCSAC-SnO_2 nanocomposite possesses a specific surface area of 36.951 m^2/g and a pore volume of 0.113 cc/g with an average pore diameter of 3.718 nm. The total pore volumes were obtained at a relative pressure of about 0.99. In Fig. 10, a distinct hysteresis loop can be seen at relative pressures of 0.4 – 1.0 suggesting the presence of a mesoporous structure and a relatively high surface area. The BET analysis results revealed the CCSAC-SnO_2 nanocomposite is suitable for a three-component reaction. The mesoporous properties should allow for efficient adsorption, diffusion, and response of the multiple substrates, leading to potentially high catalytic efficiency.

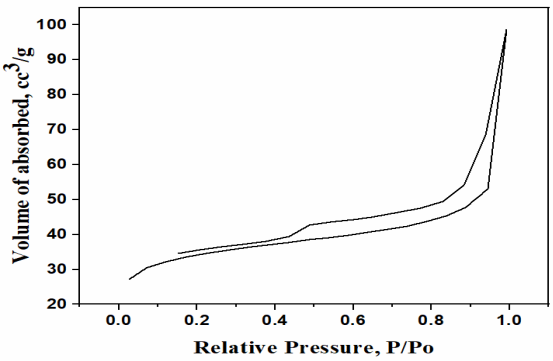

Fig. 10. N_2 adsorption-desorption isotherms of CCSAC-SnO_2 nanocomposite

The nitrogen isotherms were consistent with the representative type IV isotherm, which suggested the existence of mesopores in carbon-supported tin oxide [66].

4.7. XPS analysis of CCSAC-SnO_2 nanocomposite

The XPS spectra in Fig. 11 a show the existence of C, O, and Sn, indicating the presence of three elements in the CCSAC-SnO_2 nanocomposite. Fig. 11 b shows C 1s deconvoluted spectra of carbon-supported tin oxide. The binding energies at 284.7 eV are due to C=C [67]. The peak located at 281.4 eV with low binding energy indicates the

formation of the C-Sn bond in the CCSAC-SnO_2 nanocomposite. The peak is located at around 533.2 eV and is assigned to the O 1s (Fig. 11 c). Specifically, the core-level XPS of Sn for CCSAC-SnO_2 nanocomposite shows the presence of Sn $3d_{5/2}$ (487.3 eV) and Sn $3d_{3/2}$ (495.8 eV) (Fig. 11 d), which is contributed to Sn (IV). Moreover, the binding energy of Sn $3d_{5/2}$ is centered at 487.5 eV, which is assigned to Sn^{4+} in SnO_2 [68].

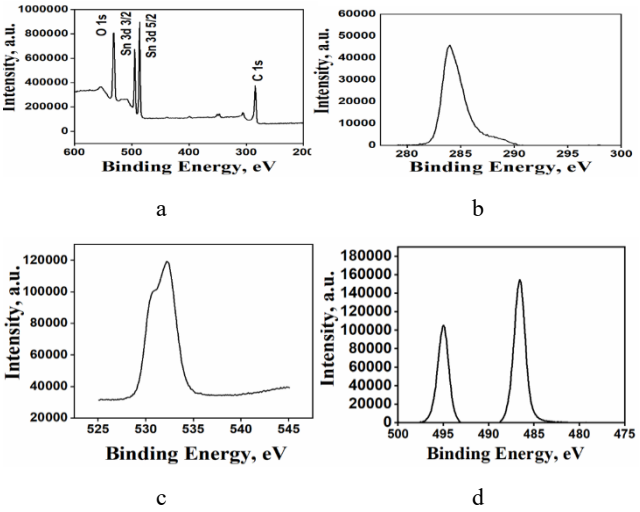

Fig. 11. XPS spectra of CCSAC-SnO_2 nanocomposite: a – full XPS spectrum; b – C 1 s; c – O1s; d – Sn 3d

4.8. TG-DTA of CCSAC-SnO_2 nanocomposite

TG-DTA, as shown in Fig. 12 a, was used to investigate the thermal properties and texture properties of the prepared CCSAC-SnO_2 nanocomposite in argon gas.

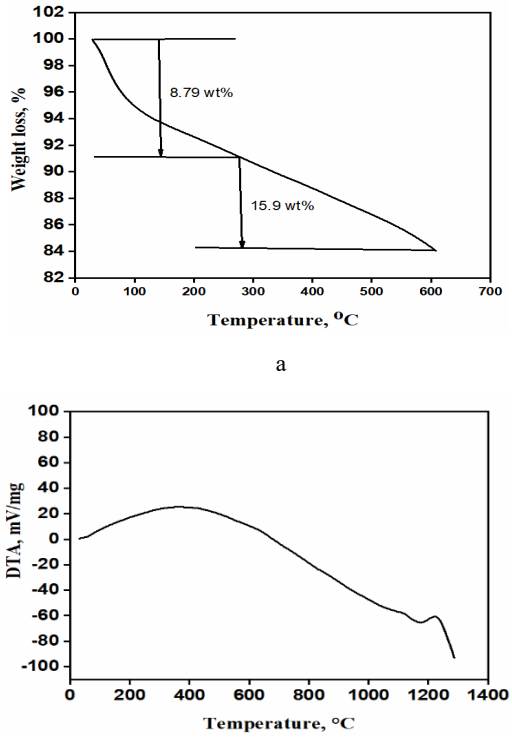

Fig. 12. a – TG analysis of CCSAC-SnO_2 nanocomposite; b – DTG analysis of CCSAC-SnO_2 nanocomposite

Water loss was observed between 0 – 300 °C and carbon decomposition of CCSAC was noted after a drastic weight loss of 15.9 wt.% at 600 °C. Thus, the content of SnO_2 in the composites is evaluated to be 84.1 wt.%. [69]. In Fig. 12 b, the DTA curve showed an exothermic peak at 378 °C, which is accompanied by a weight loss of 8.79 % that is related to the evolution of volatile components by thermal decomposition of CCSAC [70].

4.9. The catalytic activity of CCSAC-SnO_2 nanocomposite

CCSAC-SnO_2 nanocomposite was used as a nanocatalyst for the reaction involving 4-nitrobenzaldehyde, malononitrile, and dimedone in ethanol under refluxed conditions (Fig. 13). A background reaction was examined with 4-nitro benzaldehyde, malononitrile, and dimedone in the absence of CCSAC-SnO_2, resulting in no expected product formation. In this context, the solid CCSAC-SnO_2 nanocomposite nanocatalyst was used as a substitute for conventional methods for this three-component reaction. Parameters such as amount of catalyst, effect of temperature, and effect of solvents were optimized to achieve the maximum catalytic activity and good conversion of the desired product. The synthesized compound 4 was confirmed by ^{1}H NMR, as shown in Fig. 14.

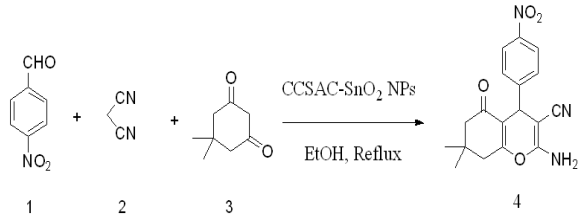

Fig. 13. The CCSAC-SnO_2 nanocomposite catalyzed the three-component synthesis of 2-amino-7,7-dimethyl-4-(4-nitrophenyl)-5-oxo-5,6,7,8-tetrahydro-4H-chromene-3-carbonitrile

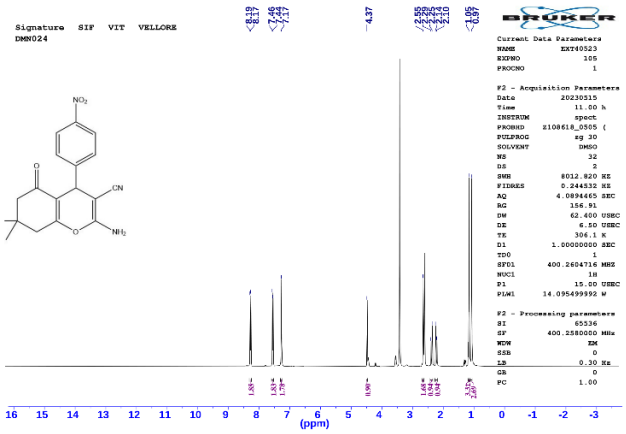

Fig. 14. ^{1}H NMR spectrum of 2-amino-7,7-dimethyl-4-(4-nitrophenyl)-5-oxo-5,6,7,8-tetrahydro-4H-chromene-3-carbonitrile

4.10. Effect of the catalyst amount, solvent, and temperature on the synthesis of 4

The effect of the catalyst amount, solvent, and temperature on the preparation of product 4 under different

reaction conditions is illustrated (scheme 1, Table 1). The temperature effect was studied across various temperature ranges, from room temperature to reflex conditions. It was observed that increasing the temperature results in higher product yields and reduced reaction time. In the case of ethanol reflux, only a trace amount of yield was obtained (entry 1). The amount of catalyst and different temperatures were optimized (entry 10 – 19). As shown in Table 1, at a lower catalyst amount of 0.1 mg, only 47 % conversion of the product was achieved after 120 min (entry 10). Increasing the catalyst amount to 0.2 mg yielded only 61 % conversion after 120 min (entry 11) while, 0.3 mg, resulted in 68 % conversion after the same duration (entry 12). An increased amount of catalyst and the temperature provided more catalytically active sites leads to increased conversion of product.

Table 1. Effect of the catalyst amount, solvent, and temperature on the synthesis of product 4

Entry	Catalyst, mg	Solvent	T, °C	Time, min	Yield, %
1	No catalyst	Ethanol	Reflux	90	trace
2	0.1	Ethanol	RT	150	35
3	0.1	Water	RT	200	23
4	0.1	toluene	RT	350	20
5	0.1	Ethyl acetate	RT	400	14
6	0.1	acetonitrile	RT	450	18
7	0.1	DMSO	RT	320	20
8	0.1	Chloroform	RT	250	30
9	0.1	Methanol	RT	189	40
10	0.1	Ethanol	RT	120	47
11	0.2	Ethanol	RT	120	51
12	0.3	Ethanol	RT	120	58
13	0.1	Ethanol	45	120	65
14	0.2	Ethanol	45	90	75
15	0.3	Ethanol	45	112	78
16	0.1	Ethanol	65	120	81
17	0.2	Ethanol	65	90	86
18	0.3	Ethanol	65	112	87
19	0.4	Ethanol	65	112	87
20	0.1	Ethanol	Reflux	45	83
21	0.2	Ethanol	Reflux	35	91
22	0.3	Ethanol	Reflux	20	96
T = temperature					

However, when the catalyst amount exceeded 0.4 mg, no noticeable change in conversion was observed (entry 19). The reaction was also performed in various solvents including ethanol (EtOH), methanol (MeOH), acetonitrile (CH_3CN), dichloromethane (CH_2Cl_3), ethyl acetate, toluene, and DMSO (entries 2 – 9). Table 1, indicated that good yield was achieved at reflex condition was found as 0.3 mg in ethanol. Additionally, experiments with different amounts of catalysts at reflux conditions demonstrated favorable yields (entry 19 – 22), with an optimum condition resulting in the highest yield and short reaction time observed in entry 22. Due to the acidic properties of tin oxide combined with its mesoporous structure, the 2 nm CCSAC-SnO_2 nanocatalyst offers a greater number of accessible sites [71]. It increased the catalytic efficiency, enabling faster turnover and improved reaction conversion, resulting in higher yields. Additionally, the temperature increased, and the reaction yield increased with less time.

4.11. Catalytic reusability of CCSAC-SnO_2 nanocomposite

The reusability of the CCSAC-SnO_2 nanocatalyst was measured through the three-component reaction of 4-nitro benzaldehyde (1) (1 mmol), malononitrile (2) (1.06 mmol), and dimedone (1 mmol) in 2 mL ethanol under refluxed conditions and stirring (CCSAC-SnO_2 nanocomposite/0.3 mg as a catalyst). The formation of product 4 was monitored by TLC. After completion of the reaction, 5 mL of hot ethanol was added to the reaction mixture and then filtered to separate catalysts. The obtained catalyst was washed several times with ethanol and dried at 100 °C. The nanocatalyst was used for 10 cycles, and results showed an insignificant loss of catalytic efficiency from 98 to 88 %.

4.12. Possible mechanism of reaction

A proposed mechanism for forming product 4 in the presence of CCSAC-SnO_2 nanocomposite is shown in Fig. 15. The Knoevenagel condensation occurs between malononitrile and activated aldehyde, resulting removal of water molecules. This process generates an intermediate of arylidenemalononitrile (intermediate I). In the next step, the tautomerization of dimedone to form enolized dimedone (II) reacts with the arylidenemalononitrile intermediate (I) (as a Michael acceptor) to form product (III). Ultimately, intramolecular cyclization and rearrangement occur, leading to the formation of product 4.

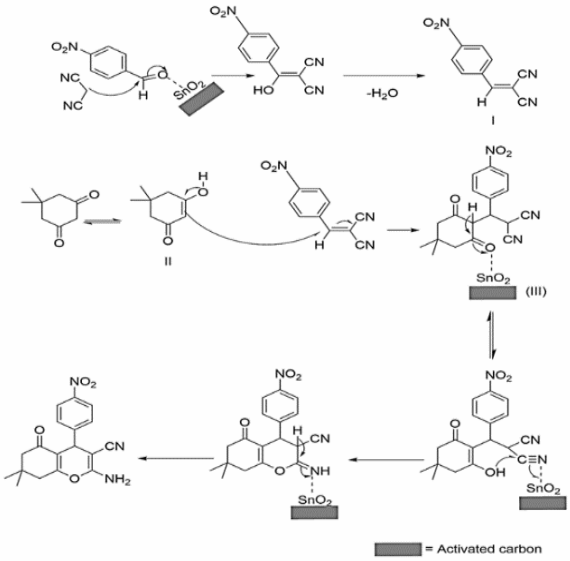

Fig. 15. Possible mechanism of reaction

5. CONCLUSIONS

The mesoporous activated carbon was prepared from the stem of *Cyperus corymbosus* a sustainable source. The CCSAC-SnO_2 nanocomposite was prepared using a green protocol with root extract from *Ruellia tuberosa*. The prepared CCSAC-SnO_2 nanocomposites were characterized by FT-IR, XRD, FE-SEM, EDX, Raman, BET, XPS, and TG-DTA. CCSAC contains crystalline carbon with an

amorphous hexagonal phase with an average nanocomposite size is about 7 nm. The prepared CSAC-SnO_2 nanocomposite average grain size of approximately 2 nm. FE-SEM images revealed that the CCSAC-SnO_2 nanocomposite was spherical with aggregated fish scale-shaped carbon. The CCSAC-SnO_2 nanocomposite demonstrated a specific surface area of 36.951 m^2/g, a pore volume of 0.113 cc/g, and an average pore diameter of 3.718 nm, indicating is mesoporous. TG-DTA analysis confirmed the high thermal stability of the prepared CCSAC-SnO_2 nanocomposite. The CCSAC-SnO_2 nanocomposite serves as a reusable, cheap nanocatalyst derived from agro-waste. Consequently, it was applied to the three-component reaction, demonstrating efficacy as a heterogeneous nanocatalyst with a yield of 96 % yield under reflux conditions and high purity within a minimal time frame, using a greener solvent.

Acknowledgments

We thank the Central Instrumentation Facility (SAPTARSHI), IIT, Jammu, India, Sophisticated Analytical Instrumentation Centre (SAIC), Tezpur University, Assam, India, Material Analysis and Research Centre, Bengaluru, and SAIF, IIT, Roorkee, India for providing instrument facilities. White solid, m.p. 175 -178 °C. 2-amino-7,7-dimethyl-4-(4-nitrophenyl)-5-oxo-5,6,7,8-tetrahydro-4H-chromene-3-carbonitrile: ^{1}H NMR (400 MHz, DMSO-d6) δ 8.18 (d, J = 8.4 Hz, 2H), 7.45 (d, J = 8.3 Hz, 2H), 7.17 (s, 2H), 4.37 (s, 1H), 2.55 (s, 2H), 2.27 (d, J = 16.1 Hz, 1H), 2.12 (d, J = 16.1 Hz, 1H), 1.05 (s, 3H), 0.97 (s, 3H).

REFERENCES

1. **Wang, H., Yu, W., Shi, J., Mao, N., Chen, S., Liu, W.** Biomass Derived Hierarchical Porous Carbons as High-Performance Anodes for Sodium-Ion Batteries *Electrochimica Acta* 188 2016: pp. 103 – 110. https://doi.org/10.1016/j.electacta.2015.12.002
2. **Wang, H., Li, Z., Tak, J.K., Holt, C.M., Tan, X., Xu, Z., Amirkhiz, B.S., Harfield, D., Anyia, A., Stephenson, T., Mitlin, D.** Supercapacitors Based on Carbons With Tuned Porosity Derived from Paper Pulp Mill Sludge Biowaste *Carbon* 57 2013: pp. 317 – 328. https://doi.org/10.1016/j.carbon.2013.01.079
3. **Julkapli, N.M., Bagheri, S.** Graphene Supported Heterogeneous Catalysts: An Overview *In International Journal of Hydrogen Energy* 40 (2) 2015: pp. 948 – 979. https://doi.org/10.1016/j.ijhydene.2014.10.129
4. **Yuan, K., Hu, T., Xu, Y., Graf, R., Brunklaus, G., Forster, M., Chen, Y., Scherf, U.** Engineering the Morphology of Carbon Materials: 2D Porous Carbon Nanosheets for High-Performance Supercapacitors *ChemElectroChem* 3 (5) 2016: pp. 822 – 828. https://doi.org/10.1002/celc.201500516
5. **Wang, H., Yu, W., Shi, J., Mao, N., Chen, S., Liu, W.** Biomass-Derived Hierarchical Porous Carbons as High-Performance Anodes for Sodium-Ion Batteries *Electrochimica Acta* 188 2016: pp. 103 – 110. https://doi.org/10.1016/j.electacta.2015.12.002
6. **Fan, X., Zhang, F.** Multiple Roles of Graphene *Chemical Society Reviews* 40 (10) 2015: pp. 3032 – 3035. https://doi.org/10.1039/C5CS00094G
7. **Gong, Y., Li, M., Li, H., Wang, Y.** Graphitic Carbon Nitride Polymers: Promising Catalysts or Catalyst Supports for Heterogeneous Oxidation and Hydrogenation *Green Chemistry* 17 (2) 2015: pp. 715 – 736. https://doi.org/10.1039/c4gc01847h
8. **Dodamani, S., Jalalpure, S., Dixit, S.R., Joshi, S.D., Vinay, A.** Synthesis, Characterization, and Molecular Docking Studies of Substituted 4-Coumarinylpyrano[2,3-C]Pyrazole Derivatives as Potent Antibacterial and Anti-Inflammatory Agents *European Journal of Medicinal Chemistry* 125 2016: pp. 101 – 116. https://doi.org/10.1016/j.ejmech.2016.09.021
9. **Klechikov, A., Mercier, G., Sharifi, T., Baburin, I.A., Seifert, G., Talyzin, A.V.** Hydrogen Storage in High Surface Area Graphene Scaffolds *Chemical Communications* 51 2015: pp. 15280 – 15283.
10. **Qian, Y., Ismail, I.M., Stein, A.** Ultralight, High-Surface-Area, Multifunctional Graphene-Based Aerogels from Self-Assembly of Graphene Oxide and Resol *Carbon* 68 2014: pp. 221 – 231. https://doi.org/10.1016/j.carbon.2013.10.082
11. **Harikrishna, S., Robert, A.R., Ganja, H., Maddila, S., Jonnalagadda, S.B.** A Green, Facile, and Recyclable Mn_3O_4/MWCNT Nano-Catalyst for the Synthesis of Quinolines Via One-Pot Multicomponent Reactions *Sustainable Chemistry and Pharmacy* 16 2020: pp. 100265. https://doi.org/10.1016/j.scp.2020.100265
12. **Yadav, J.S., Reddy, V.S., Sridhar, P., Reddy, J.S.S., Nagaiah, K., Lingaiah, N., Saiprasad, P.S.** Green Protocol for the Biginelli Three-Component Reaction : $Ag_3PW_{12}O_{40}$ as a Novel, Water-Tolerant Heteropolyacid for the Synthesis of 3 , 4-Dihydropyrimidinones *European Journal of Organic Chemistry* 2004 (3) 2004: pp. 552 – 557. https://doi.org/10.1002/ejoc.200300559
13. **El-yazeed, W.S.A., Awad, M.E., Amr, I.A., Ibrahim, A.** Fluorine-Doped Tin Oxide as Efficient Solid Acid Catalyst : Acidity and the Catalytic Activity Relationship *Journal of Sol-Gel Science and Technology* 97 2021: pp:191 – 204. https://doi.org/10.1007/s10971-020-05422-9
14. **Okuhara, T.** Water-Tolerant Solid Acid Catalysts *Chemical Reviews* 102 2002: pp. 3641 – 3666. https://doi.org/10.1021/cr0103569
15. **Pavlovic, J., Popova, M., Mihalyi, R.M., Mazaj, M., Mali, G., Kovač, J., Lazarova, H., Rajic, N.** The Catalytic Activity of Sno_{2-} And SO_4/SnO_2-Containing Clinoptilolite in the Esterification of Levulinic Acid *Microporous and Mesoporous Materials* 279 2019: pp. 10 – 18. https://doi.org/10.1016/j.micromeso.2018.12.009
16. **Harikrishna, S., Robert, A.R., Ganja, H., Maddila, S., Jonnalagadda, S.B.** A Green, Facile and Recyclable Mn_3O_4/MWCNT Nano-Catalyst for the Synthesis of Quinolines Via One-Pot Multicomponent Reactions *Sustainable Chemistry and Pharmacy* 16 2020: pp. 100265. https://doi.org/10.1016/j.scp.2020.100265
17. **Al-hamdi, A.M., Sillanpää, M., Bora, T., Dutta, J.** Efficient Photocatalytic Degradation of Phenol in Aqueous Solution By SnO_2:Sb Nanoparticles *Applied Surface Science* 370 2016: pp. 229 – 236. https://doi.org/10.1016/j.apsusc.2016.02.123
18. **Lee, D., Wan, Z., Bae, J., Lee, H., Ahn, J., Kim, S., Kim, J., Kwon, S.** Plasma-Enhanced Atomic Layer Deposition of SnO_2 Thin Films Using $SnCl_4$ and O_2 Plasma *Materials Letters* 166 2016: pp. 163 – 166. https://doi.org/10.1016/j.matlet.2015.12.049
19. **Rahal, A., Benhaoua, A., Jlassi, M., Benhaoua, B.** Structural, Optical, and Electrical Properties Studies of

Ultrasonically Deposited Tin Oxide (SnO_2) Thin Films With Different Substrate Temperatures *Superlattices and Microstructures* 86 2015: pp. 403 – 411. https://doi.org/10.1016/j.spmi.2015.08.003

20. **Subramani, C., Chandrabose, M.** SnO_2 Nanoparticles as an Efficient Heterogeneous Catalyst for the Synthesis of 2 H - Indazolo [2,1-B] Phthalazine-Triones *Journal of Nanostructure in Chemistry* 7 2017: pp. 283 – 291. https://doi.org/10.1007/s40097-017-0238-1
21. **Ganthi, S.** Indigenous Knowledge on Natural Dyeing of Korai Grass Mat In Pattamadai, Tirunelveli District, Tamil Nadu *Natural Product Radiance* 8 (5) 2009: pp. 542 – 545.
22. **Malathi, A., Lethi, C.D., Ilangovan, S.** Composting of Korai Grass (Cyperus Corymbosus Rottb.) Waste by Native Microbe and Earthworm Species in Ayyampalayam, Tiruchirappalli District, Tamilnadu, India *Indian Journal of Natural Sciences* 4 (22) 2014: pp. 1465 – 1473.
23. **Akimoto, H.** Global Air Quality And Pollution *Science* 302 (5651) 2003: pp. 1716 – 1719. https://doi.org/10.1126/science.1092666
24. **Yu, B., Li, Y., Wang, Y., Li, H., Zhang, R.** Journal of Environmental Chemical Engineering Facile Hydrothermal Synthesis of SnO_2 Quantum Dots with Enhanced Photocatalytic Degradation Activity: Role of Surface Modification with Chloroacetic Acid *Journal of Environmental Chemical Engineering* 9 (4) 2021: pp. 105618. https://doi.org/10.1016/j.jece.2021.105618
25. **Abdelkader, E., Nadjia, L., Rose-noe, V.** Adsorption of Congo Red Azo Dye on Nanosized SnO_2 Derived from the Sol-Gel Method *International Journal of Industrial Chemistry* 7 2015: pp. 53 – 70. https://doi.org/10.1007/s40090-015-0061-9
26. **Ma, C.M., Hong, G.B., Lee, S.C.** Facile Synthesis of Tin Dioxide Nanoparticles for Photocatalytic Degradation of Congo Red Dye in Aqueous Solution *Catalysts* 10 (7) 2020: pp. 1 – 17. https://doi.org/10.3390/catal10070792
27. **Davar, F., Salavati-niasari, M., Fereshteh, Z.** Synthesis and Characterization of SnO_2 Nanoparticles by Thermal Decomposition of New Inorganic Precursor *Journal of Alloys and Compounds* 496 (1 – 2) 2010: pp. 638 – 643. https://doi.org/10.1016/j.jallcom.2010.02.152
28. **Chakravarty, R., Chakraborty, S., Shukla, R., Bahadur, J., Ram, R., Mazumder, S., Sarma, H.D., Tyagi, A.K., Dash, A.** Mechanochemical Synthesis of Mesoporous Tin Oxide : A New Generation Nanosorbent for 68Ge/68Ga Generator Technology *Dalton Transactions* 45 (34) 2016: pp. 13361 – 13372. https://doi.org/10.1039/c6dt01921h
29. **Zamand, N., Pour, A.N., Housaindokht, M.R., Izadyar, M.** Size-Controlled Synthesis of SnO_2 Nanoparticles Using Reverse Microemulsion Method *Solid State Sciences* 33 2014: pp. 6 – 11. https://doi.org/10.1016/j.solidstatesciences.2014.04.005
30. **Mittal, A.K., Chisti, Y., Banerjee, U.C.** Synthesis of Metallic Nanoparticles Using Plant Extracts *Biotechnology Advances* 31 (2) 2013: pp. 346 – 356. https://doi.org/10.1016/j.biotechadv.2013.01.003
31. **Chandrasekaran, R., Gnanasekar, S., Seetharaman, P., Keppanan, R., Arockiaswamy, W., Sivaperumal, S.** Formulation of Carica Papaya Latex-Functionalized Silver Nanoparticles for its Improved Antibacterial and Anticancer Applications *Journal of Molecular Liquids* 219 2016: pp. 232 – 238. https://doi.org/10.1016/j.molliq.2016.03.038
32. **Ahmed, S., Ahmad, M., Swami, B.L., Ikram, S.** A Review on Plants Extract Mediated Synthesis of Silver Nanoparticles for Antimicrobial Applications : A Green Expertise *Journal of Advanced Research* 7 (1) 2016: pp. 17 – 28. https://doi.org/10.1016/j.jare.2015.02.007
33. **Qu, J., Yuan, X., Wang, X., Shao, P.** Zinc Accumulation and Synthesis of ZnO Nanoparticles Using Physalis Alkekengi L *Environmental Pollution* 159 (7) 2011: pp. 1783 – 1788. https://doi.org/10.1016/j.envpol.2011.04.016
34. **Heinlaan, M., Ivask, A., Blinova, I., Dubourguier, H., Kahru, A.** Toxicity of Nanosized and Bulk ZnO, CuO and TiO_2 to Bacteria Vibrio Fischeri and Crustaceans Daphnia Magna and Thamnocephalus Platyurus *Chemosphere* 71 2008: pp. 1308 – 1316. https://doi.org/10.1016/j.chemosphere.2007.11.047
35. **Dömling, A.** Recent Developments in Isocyanide Based Multicomponent Reactions in Applied Chemistry *Chemical Reviews* 106 (1) 2006: pp. 17 – 89.
36. **Ma, C., Yang, Y.** Thiazolium-Mediated Multicomponent Reactions: A Facile Synthesis of 3-Aminofuran Derivatives *Organic Letters* 6 2005: pp. 2004 – 2006.
37. **Bhunia, A., Yetra, S.R., Gonnade, R.G., Biju, A.T.** Synthesis of 4 H-Chromenes by an Unexpected, K_3PO_4-Mediated Intramolecular Rauhut–Currier Type Reaction *Organic & Biomolecular Chemistry* 14 (24) 2016: pp. 5612 – 5616. https://doi.org/10.1039/C6OB00654J
38. **Khafagy, M.M., Abd El-Wahab, A.H., Eid, F.A., El-Agrody, A.M.** Synthesis of Halogen Derivatives of Benzo[H]Chromene and Benzo [A] Anthracene with Promising Antimicrobial Activities *II Farmaco* 57 (9) 2002: pp. 715 – 722. https://doi.org/10.1016/S0014-827X(02)01263-6
39. **Flavin, M.T., Rizzo, J.D., Khilevich, A., Kucherenko, A., Sheinkman, A.K., Vilaychack, V., Lin, L., Chen, W., Greenwood, E.M., Pengsuparp, T., Pezzuto, J.M., Hughes, S.H., Flavin, T.M., Cibulski, M., Boulanger, W.A., Shone, R.L.** Synthesis, Chromatographic Resolution, and Anti-Human Immunodeficiency Virus Activity of (±)-Calanolide A and its Enantiomers *Journal of Medicinal Chemistry* 39 (6) 1996: pp. 1303 – 1313.
40. **Kemnitzer, W., Drewe, J., Jiang, S., Zhang, H., Zhao, J., Crogan-grundy, C., Xu, L., Tseng, B., Kasibhatla, S., Cai, S.X.** Discovery of 4-Aryl-4 H-Chromenes as a New Series of Apoptosis Inducers Using a Cell and Caspase-Based High-Throughput Screening Assay. 3. Structure − Activity Relationships of Fused Rings at the 7, 8-Positions *Journal of Medicinal Chemistry* 50 (12) 2007: pp. 2858 – 2864.
41. **Ranjith, R., Perumal, S., Menéndez, J.C., Yogeeswari, P.** Bioorganic & Medicinal Chemistry Hybrids Generated by Chemoselective 1, 3-Dipolar Cycloadditions of Nitrile Oxides *Bioorganic & Medicinal Chemistry* 19 (11) 2011:pp. 3444 – 3450. https://doi.org/10.1016/j.bmc.2011.04.033
42. **Mirjalili, B.B.F., Zamani, L., Zomorodian, K., Khabnadideh, S., Haghighijoo, Z., Malakotikhah, Z., Mousavi, S.A.A., Khojasteh, S.** Synthesis, Antifungal Activity and Docking Study of 2-Amino-4H-Benzochromene-3-Carbonitrile Derivatives *Journal of Molecular Structure* 1116 2016: pp. 102 – 108. https://doi.org/10.1016/j.molstruc.2016.03.002
43. **Kumar, D., Reddy, V.B., Sharad, S., Dube, U., Kapur, S.**

A Facile One-Pot Green Synthesis and Antibacterial Activity Tetrahydro-4 H -Chromenes *European Journal of Medicinal Chemistry* 44 (9) 2009: pp. 3805 – 3809. https://doi.org/10.1016/j.ejmech.2009.04.017

44. **Davoodnia, A., Allameh, S., Fazli, S., Tavakoli-hoseini, N.** One-Pot Synthesis of 2-Amino-3-Cyano-4-Arylsubstituted Tetrahydrobenzo[B]Pyrans Catalysed by Silica Gel-Supported Polyphosphoric Acid (PPA – SiO_2) as an Efficient and Reusable Catalyst *Chemical Papers* 65 (5) 2011: pp. 714 – 720. https://doi.org/10.2478/s11696-011-0064-8
45. **Wang, X.S., Shi, D.Q., Tu, S.J., Yao, C.S.** A Convenient Synthesis of 5-Oxo-5,6,7,8-Tetrahydro-4H-Benzo-[B]-Pyran Derivatives Catalyzed By KF-Alumina *Synthetic Communications* 31(1) 2013: pp. 37 – 41. https://doi.org/10.1081/SCC-120015567
46. **Davoodnia, A., Allameh, S., Fazli, S., Tavakoli-hoseini, N.** One-Pot Synthesis of 2-Amino-3-Cyano-4-Arylsubstituted Tetrahydrobenzo[B]Pyrans Catalysed by Silica Gel-Supported Polyphosphoric Acid (PPA – SiO_2) as an Efficient and Reusable Catalyst *Chemical Papers* 65 (5) 2011: pp. 714 – 720. https://doi.org/10.2478/s11696-011-0064-8
47. **Synthesi, A.C.O.** A Clean One-Pot Synthesis of Tetrahydrobenzo[B]Pyran Derivatives Catalyzed by Hexadecyltrimethyl Ammonium Bromide in Aqueous Media *Chemical Papers* 65 2004: pp. 871 – 873. https://doi.org/10.1055/s-2004-820025
48. **Rostami, A., Atashkar, B., Gholami, H.** Novel Magnetic Nanoparticles Fe_3O_4-Immobilized Domino Knoevenagel Condensation, Michael Addition, and Cyclization Catalyst *Catalysis Communications* 37 2013: pp. 69 – 74. https://doi.org/10.1016/j.catcom.2013.03.022
49. **Aswin, K., Mansoor, S.S., Logaiya, K., Sudhan, S.P.N., Malik, V.S., Ramadoss, H.** Reusable Silica-Bonded S-Sulfonic Acid Catalyst for Three-Component Synthesis of 2-Amino-5-Oxo-5, 6, 7, 8-Tetrahydro-4 H-Chromenes and 2-Amino-4 H-Pyrans in Aqueous Ethanol *Research on Chemical Intermediates* 40 2014: pp. 2589 – 2598. https://doi.org/10.1007/s11164-013-1111-6
50. **Seifi, M., Sheibani, Æ.H.** High Surface Area MgO as a Highly Effective Heterogeneous Base Catalyst for Three-Component Synthesis of Tetrahydrobenzopyran and 3 , 4-Dihydropyrano[C]Chromene Derivatives in Aqueous Media *Catalysis Letters* 126 2008: pp. 275 – 279. https://doi.org/10.1007/s10562-008-9603-5
51. **Rahnamafa, R., Moradi, L., Khoobi, M.** Rapid and Green Synthesis of 4H-Benzo [B] Pyrans Using Triethanolamine as an Efficient Homogeneous Catalyst under Ambient Conditions *Research on Chemical Intermediates* 46 2020: pp. 2109 – 2116. https://doi.org/10.1007/s11164-020-04081-3
52. **Kaur, R., Naaz, F., Sharma, S., Mehndiratta, S., Kumar, M.** Screening of a Library of 4-Aryl/Heteroaryl-4 H-Fused Pyrans for Xanthine Oxidase Inhibition: Synthesis, Biological Evaluation and Docking Studies *Medicinal Chemistry Research* 24 2015: pp. 3334 – 3349. https://doi.org/10.1007/s00044-015-1382-0
53. **Behbahani, F.K., Alipour, F.** One-Pot Synthesis of 2-Amino-4 H -Pyrans and 2-Amino-Tetrahydro-4 H-Chromenes Using L -Proline *Gazi University Journal of Science* 28 (3) 2015: pp. 387 – 393.
54. **Yaghoubi, A., Dekamin, M.G.** Green And Facile Synthesis of 4 H -Pyran Scaffold Catalyzed by Pure Nano-Ordered Periodic Mesoporous Organosilica with Isocyanurate Framework (PMO-ICS) *ChemistrySelect* 2 (28) 2017: pp. 9236 – 9243. https://doi.org/10.1002/slct.201700717
55. **Zhang, T., Jin, H., Fang, Y., Guan, J., Ma, S., Pan, Y., Zhang, M., Zhu, H., Liu, X., Du, M.** Detection of Trace Cd2+, Pb2+ and Cu2+ Ions Via Porous Activated Carbon Supported Palladium Nanoparticles Modified Electrodes Using SWASV *Materials Chemistry and Physics* 225 2019: pp. 443 – 442. https://doi.org/10.1016/j.matchemphys.2019.01.010
56. **Gomathi, E., Jayapriya, M., Arulmozhi, M.** Environmental Benign Synthesis of Tin Oxide (SnO_2) Nanoparticles Using Actinidia Deliciosa (Kiwi) Peel Extract with Enhanced Catalytic Properties *Inorganic Chemistry Communications* 130 2021: pp. 108670. https://doi.org/10.1016/j.inoche.2021.108670
57. **Ghorbani, F., Kamari, S., Zamani, S., Akbari, S., Salehi, M.** Optimization and Modeling of Aqueous Cr(VI) Adsorption onto Activated Carbon Prepared From Sugar Beet Bagasse Agricultural Waste by Application of Response Surface Methodology *Surfaces and Interfaces* 18 2020: pp. 100444. https://doi.org/10.1016/j.surfin.2020.100444
58. **Dziejarski, B., Junior, O.F.C.** Design of Highly Microporous Activated Carbons Based on Walnut Shell Biomass for H_2 and CO_2 Storage *Carbon* 201 2023: pp. 633 – 647.
59. **Bhattacharjee, A., Sinha, T.** Surfactant Effects on the Synthesis of Durable Tin-Oxide Nanoparticles and its Exploitation as a Recyclable Catalyst for the Elimination of Toxic Dye: A Green and Efficient Approach for Wastewater Treatment *RSC Advances* 4 2014: pp. 51418 – 51429. https://doi.org/10.1039/C4RA08461F
60. **Lima, S.B., Borges, S.M.S., Marchetti, S.G.** Effect of Iron Content on the Catalytic Properties of Activated Carbon-Supported Magnetite Derived from Biomass *Journal of the Brazilian Chemical Society* 24 (2) 2013: pp. 344 – 354. https://doi.org/10.5935/0103-5053.20130044
61. **Mishra, S., Singh, S., Rawat, S., Singh, J.** Corn Husk Derived Magnetized Activated Carbon for The Removal of Phenol and Para-Nitrophenol from Aqueous Solution: Interaction Mechanism, Insights on Adsorbent Characteristics, and Isothermal, Kinetic and Thermodynamic Properties *Journal of Environmental Management* 246 2019: pp. 362 – 373. https://doi.org/10.1016/j.jenvman.2019.06.013
62. **Ha, H., Hung, P., Cao, V.H., Tuan, L., Tran, V.M.** SnO_2 Nanosheets/Graphite Oxide/G-C_3N_4 Composite as Enhanced Performance Anode Material for Lithium Ion Batteries *Chemical Physics Letters* 715 2019: pp. 284 – 292. https://doi.org/10.1016/j.cplett.2018.11.052
63. **Fernández Honaine, M., Zucol, A.F., Osterrieth, M.L.** Phytolith Analysis of Cyperaceae from the Pampean Region, Argentina *Australian Journal of Botany* 57 2009: pp. 512 – 523. https://doi.org/10.1071/BT09041
64. **Scott, J.F.** Raman Spectrum of SnO_2 *The Journal of Chemical Physics* 852 – 853 1970: pp. 16 – 18. https://doi.org/10.1063/1.1674079
65. **Zhou, J.X., Zhang, M.S., Hong, J.M., Yin, Z.** Raman Spectroscopic and Photoluminescence Study of Single-Crystalline Sno_2 Nanowires *Solid State Communications* 138 2006: pp. 242 – 246. https://doi.org/10.1016/j.ssc.2006.03.007
66. **He, X., Liu, Y., Wang, Q., Wang, T., He, J., Peng, A.,**

Qi, K. Facile Fabrication of Eu – Based Metal – Organic Frameworks for Highly Efficient Capture of Tetracycline Hydrochloride from Aqueous Solutions *Scientific Reports* 13 (1) 2023: pp. 1 – 13. https://doi.org/10.1038/s41598-023-38425-x

67. **Xu, B., Wu, H., Lin, C.C., Wang, B., Zhang, Z., Zhao, X.S.** Stabilization of Silicon Nanoparticles in Graphene Aerogel Framework for Lithium Ion Storage *RSC Advances* 39 2015: pp. 30624 – 30630. https://doi.org/10.1039/C5RA00566C
68. **Tian, Q., Zhang, Z., Yang, L., Hirano, S.I.** Synthesis of SnO_2/Sn@Carbon Nanospheres Dispersed in the Interspaces of a Three-Dimensional SnO_2/Sn@Carbon Nanowires Network, and their Application as an Anode Material for Lithium-Ion Batteries *Journal of Materials Chemistry A* 2 (32) 2014: pp. 12881 – 12887. https://doi.org/10.1039/c4ta02059f
69. **Meng, J.K., Wang, W.W., Wang, Q.C., Cao, M.H., Fu, Z.W., Wu, X.J., Zhou, Y.N.** Graphene Supported Ultrafine Tin Oxide Nanoparticles Enable Conversion Reaction Dominated Mechanism for Sodium-Ion Batteries *Electrochimica Acta* 303 2019: pp. 32 – 39. https://doi.org/10.1016/j.electacta.2019.02.072
70. **Schier, L., Lima, D., Dennison, M., Araujo, M., Pércio, S.** Adsorption Modeling of Cr, Cd and Cu on Activated Carbon of Different Origins by Using Fractional Factorial Design Adsorption Modeling of Cr, Cd and Cu on Activated Carbon of Different Origins by Using Fractional Factorial Design *Chemical Engineering Journal* 166 (3) 2011: pp. 881 – 889. https://doi.org/10.1016/j.cej.2010.11.062
71. **Feng, D., Dong, Y., Zhang, L., Ge, X., Zhang, W., Dai, S., Qiao, Z.A.** Holey Lamellar High-Entropy Oxide as an Ultra-High-Activity Heterogeneous Catalyst for Solvent-Free Aerobic Oxidation of Benzyl Alcohol *Angewandte Chemie* 59 (44) 2020: pp. 19503 – 19509. https://doi.org/10.1002/anie.202004892